

# **Transmission control of VO<sub>2</sub> nanostructures by IR based 1-D Photonic crystal as hybrid Photonic absorbers**

**Dipti Umed Singh\*<sup>1</sup>, Omkar Bhoite <sup>1</sup> and Remya Narayanan\*<sup>2</sup>**

*<sup>1</sup>Department of Physics & Centre for Energy Science, Indian Institute of Science Education and Research, Pune 411008, Maharashtra, India*

*<sup>2</sup>Department of Environmental Science, Savitribhai Phule Pune University, Pune, 411007, Maharashtra, India*

**\*Corresponding authors' emails: [remyapadmaja@gmail.com](mailto:remyapadmaja@gmail.com) ; [dipti@students.iiserpune.ac.in](mailto:dipti@students.iiserpune.ac.in)**

## Abstract

The effect of 1-D photonic crystals on optical transmission of VO<sub>2</sub> is studied by depositing VO<sub>2</sub> thin films on Distributed Bragg Reflectors (DBR) in the infrared (IR) spectral range. Monoclinic VO<sub>2</sub> nanoparticles with tuned crystallinity were synthesized by a facile solution processed method. Moderately crystalline (MC) and highly crystalline (HC) VO<sub>2</sub> nanostructures were obtained by varying its synthesis temperature and annealing conditions. Both MC and HC VO<sub>2</sub> exhibit expected reduction in optical transmission in the IR region due to its structural phase transition from monoclinic (insulator) to rutile (metallic) around a critical temperature of 68 °C. By combining VO<sub>2</sub> films on 40 % transmitting DBR structure, the average optical transmission further went down to ~30 %. The number of stacks of DBR plays a key role in such effective reduction of optical transmission. When the number of stacks of DBR increased from 4 to 7, the optical transmission of metallic VO<sub>2</sub> films on DBR nearly vanishes in Near-IR spectrum in such vanadium dioxide/1D photonic crystal based composite nanostructures as per earlier theoretical predictions. Such enhanced broad band optical response can be a promising design for VO<sub>2</sub> based hybrid photonic absorbers for various smart window applications.

Keywords: Vanadium dioxide, Photonic crystal, Distributed Bragg reflector, infrared, and absorber.

## 1. Introduction

Monoclinic Vanadium dioxide VO<sub>2</sub> (M) is a prototype material which can undergo fully reversible metal to insulator transition (MIT) above a critical temperature ( $T_c$ ) of 68 °C. This phase transition occurs due to crystallographic phase change from monoclinic M (insulator or semiconducting) phase to rutile R phase (metallic) [1, 2]. Owing to this VO<sub>2</sub> exhibits predominant changes in its correlated optical and electrical properties [3, 4]. Such MIT transition also leads to abrupt changes from IR transparent semiconducting M state to infra-red (IR) blocking metallic R state, [5] with resistance changing by few orders of magnitude [6]. Such intriguing properties make VO<sub>2</sub> as a promising candidate for active optoelectronic and infrared memory devices [7] and this has been extensively used for smart window coating and IR based optical absorbers [8, 9]. VO<sub>2</sub> based metamaterials are also designed for broad band tunable terahertz absorber [10, 11]. In a

recent report, VO<sub>2</sub> was used as an active device for color rendering and IR tuning of photo detection devices [12]. Moreover Electromagnetic induced transparency was also observed in a hybrid structure consisting of VO<sub>2</sub> nanoparticles having a three level quantum dot (QD) system where VO<sub>2</sub> QDs act as an optical nano switch that changes with temperature [13].

On the other hand, 1-D photonic crystals are one of the most important yet, simple artificial structures to accomplish optical control by localizing light modes and by controlling the flow of light [14, 15]. This consists of a photonic crystal having one dimensional periodic array of multilayers of two materials with different dielectric constants having very high reflectivity called as Distributed Bragg reflector (DBR). DBR is a highly reflecting mirror with each layer is designed to have a thickness equal to the one quarter of the wavelength of the light [16, 17]. DBR based Photonic crystals are already used as a back reflector for enhanced emission from heterostructured LEDs [18] and also as a directly absorptive medium [19-21]. Such structures also play key roles in wider applications of thermophotovoltaics and IR photodetectors for energy conservation [22-25]. There were widespread applications of DBR in Bio-Sensing devices [26, 27] as well chemical sensors [28, 29] and IR imaging Device [30]. Such 1-D photonic crystal paved a new path for novel efficient hybrid design for optical absorbers across the electromagnetic spectrum. Metamaterial perfect functional absorbers based on DBR structures have already been proposed [31]. Moreover, 2D materials with 1-D photonic crystal based hybrid structures were studied for enhanced optical absorption as well as for thermal coherent source [32]. Absorption enhancement of 2D materials such as MoS<sub>2</sub> and WS<sub>2</sub> monolayers with Bragg reflector hybrid structures was already studied [33-35]. Moreover, there were a wide range of applications with graphene based structural defect inside 1D photonic crystal for non-linear control of absorption as well [36, 37]. Hence 1D Photonic crystal based hybrid structures were studied intensively in order to achieve perfect absorption due to localized photonic modes. There are recent reports of visible transmittance enhancement of VO<sub>2</sub> thin films by anti-reflection coatings [38].

In this work we have confirmed the theoretical predication of absorption enhancement of VO<sub>2</sub> nanostructure over 1-D Photonic crystal in near IR range [39, 40]. Here we have experimentally implemented a DBR based 1D photonic crystal, fabricated with SiO<sub>2</sub>/TiO<sub>2</sub> alternating structure with VO<sub>2</sub> (M) nanostructures. In this report, observed a significant reduction of optical transmission in the IR regime in such a hybrid structures. Therefore, this 1-D photonic

crystal/ $\text{VO}_2$  thin films are proposed as functional optical coating to achieve close to unit optical absorption in the IR range.

## **2. Experimental Details**

### ***2.1 Material Used***

Ammonium meta-vanadate ( $\text{NH}_4\text{VO}_3$ , 99 %, Sigma-Aldrich), ethylene glycol ( $\text{C}_2\text{H}_6\text{O}_2$ , 99.8 %, Sigma-Aldrich), Polyvinylpyrrolidone (PVP, Sigma Aldrich), Ethanol, glass microscope slides (two side polished), silicon dioxide ( $\text{SiO}_2$ ) and titanium dioxide ( $\text{TiO}_2$ ) sputtering target of 2 inch diameter, 0.25 inch thickness.

### ***2.2 Synthesis of $\text{VO}_2$ nanoparticles***

1 g of  $\text{NH}_4\text{VO}_3$  was added to 50 ml of ethylene glycol and this reaction mixture was kept at 160 °C in an oil bath for 2 hours with vigorous stirring, resulted the formation of purple color Vanadyl ethylene glycol complex (VEG). This complex was allowed to cool down to room temperature. After cooling, the complex was centrifuged several times with copious amount of ethylene glycol and ethanol to remove residues from the complex precipitate. Obtained precipitate was further dried for 4 hours at 60 °C and then heated at 190 °C for 30 minutes in a vacuum oven in an ambient atmosphere. This leads to the formation of black powder of  $\text{VO}_2$ , which is moderately crystalline (MC). This MC  $\text{VO}_2$  powder was further annealed at 650 °C for 2 hours with a ramp rate of 5 °C/minute in an Argon air flow. Before annealing, tube furnace was purged with argon gas for 30 minutes to remove the excess oxygen from the chamber to avoid oxidation of  $\text{VO}_2$  powder. The system was allowed to cool down to room temperature leading to the formation of high crystalline  $\text{VO}_2$  (HC) powder.

### ***2.3 DBR Fabrication***

$\text{SiO}_2/\text{TiO}_2$  multilayers were grown in Moorfield's Minilab ST80A magnetron Sputtering deposition system. DBR Multilayers were coated on thoroughly cleaned microscope glass slides of size  $0.5 \times 0.5 \text{ cm}^2$ . The base pressure of a sputtering chamber was kept at  $\sim 1 \times 10^{-7}$  mbar. While depositing  $\text{SiO}_2$  and  $\text{TiO}_2$ , the vacuum chamber was kept at  $9.2 \times 10^{-3}$  mbar. Thickness of  $\text{SiO}_2$  and  $\text{TiO}_2$  were calibrated using a Profilometer (Veeco, Dektak 150). Two DBRs with central wavelength of  $\lambda_0 = 1350 \text{ nm}$  and  $1600 \text{ nm}$  were fabricated respectively. For DBR with central

wavelength  $\lambda_0 = 1350$  nm, four periods of SiO<sub>2</sub>/TiO<sub>2</sub> and their thickness were chosen to be of quarter wavelength ( $d = \lambda/4n$ , where  $n$  is the refractive index of the material used). Therefore the thickness for each layer were  $t_{\text{SiO}_2} \sim 230$  nm and  $t_{\text{TiO}_2} \sim 130$  nm respectively. For DBR with central wavelength  $\lambda_0 = 1600$  nm, seven pairs of SiO<sub>2</sub>/TiO<sub>2</sub> with required thickness of  $t_{\text{SiO}_2} \sim 275$  nm and  $t_{\text{TiO}_2} \sim 150$  nm were grown respectively.

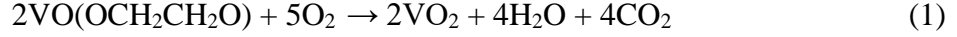
## ***2.4 Characterization Techniques***

Morphology of VO<sub>2</sub> nanostructures were investigated by field emission scanning electron microscopy (FESEM, Zeiss Ultra Plus) and by transmission electron microscope (JEOL JEM-2200FS). High resolution transmission electron microscopy (HRTEM) images and selected area diffraction (SAED) patterns were obtained by JEOL – 2200FS operating at 200 KV. Chemical compositions were analyzed by Oxford's 80 mm<sup>2</sup> EDX detector. High temperature X-ray diffraction pattern was recorded by Bruker D8 Advance X-ray diffractometer with Cu K $\alpha$  radiation (1.54 Å) with temperature ranges were from 300 K to 380 K. The two theta scanning range was from 10 to 70°. Thermochromic properties of VO<sub>2</sub> were explored with an experimental setup consisting of 1000 Watts quartz-tungsten-halogen lamp and Acton Research's SP2555i monochromator to scan wavelength range from 900-2500 nm. The samples were kept inside customized copper sample holders inside ARS CS204-DMX-20 closed cycle cryostat for temperature dependent measurements. The temperature was varied from 300 K to 380 K. Finally to record the transmission, the transmitted light passed through the sample to photodetector Thorlabs FGA20.

## **3. Result and discussion**

### ***3.1 structural and morphological analysis of VO<sub>2</sub>***

VEG complexes were obtained by the reduction of V<sup>5+</sup> in NH<sub>4</sub>VO<sub>3</sub> to V<sup>4+</sup> by pyrolysis in ethylene glycol [41]. This provides a planar sheet like morphology as shown in figure S1(a) provided in supporting information. The average length of each sheet is of a few micrometers. Thermolysis of VEG complexes leads to the formation of MC VO<sub>2</sub> in ambient atmosphere, according to the following equation.



FESEM images showing rod like morphology for as prepared MC VO<sub>2</sub> in figure 1(a). TEM images further confirm the formation of nanorods with a size distribution ranging from 100 – 200 nm and these are aggregated in clusters. It is assumed that, VEG complexes acting as a seed for VO<sub>2</sub> nanorods. The surface energy of VO<sub>2</sub> nanorods formed at ambient temperatures is relatively large and they can aggregate well together. Figure 1(c) depicts the high resolution TEM. This provides the information about the VO<sub>2</sub> crystalline phase. The calculated interplanar distance of VO<sub>2</sub> nanocrystals is around 3.2 Å, this corresponds to (011) plane of MC-VO<sub>2</sub> (M) (JCPDS: 82-0661). Post annealing of as prepared MC VO<sub>2</sub> at 650 °C resulted in the formation of HC VO<sub>2</sub> nanoparticles with uniform distribution. This morphology is consistent with previous reports in the literature. As formed HC VO<sub>2</sub> has regular and clear grain boundaries as shown in figure 1(d). Xiao *et al.* [42] reported that, when annealing temperature is increased, the surface energy of the particles with large crystalline size reduced and which leads to reduced aggregation. The calculated interplanar distance of HC VO<sub>2</sub> (M) polyhedron is 2.42 Å which corresponds to the (200) miller plane.

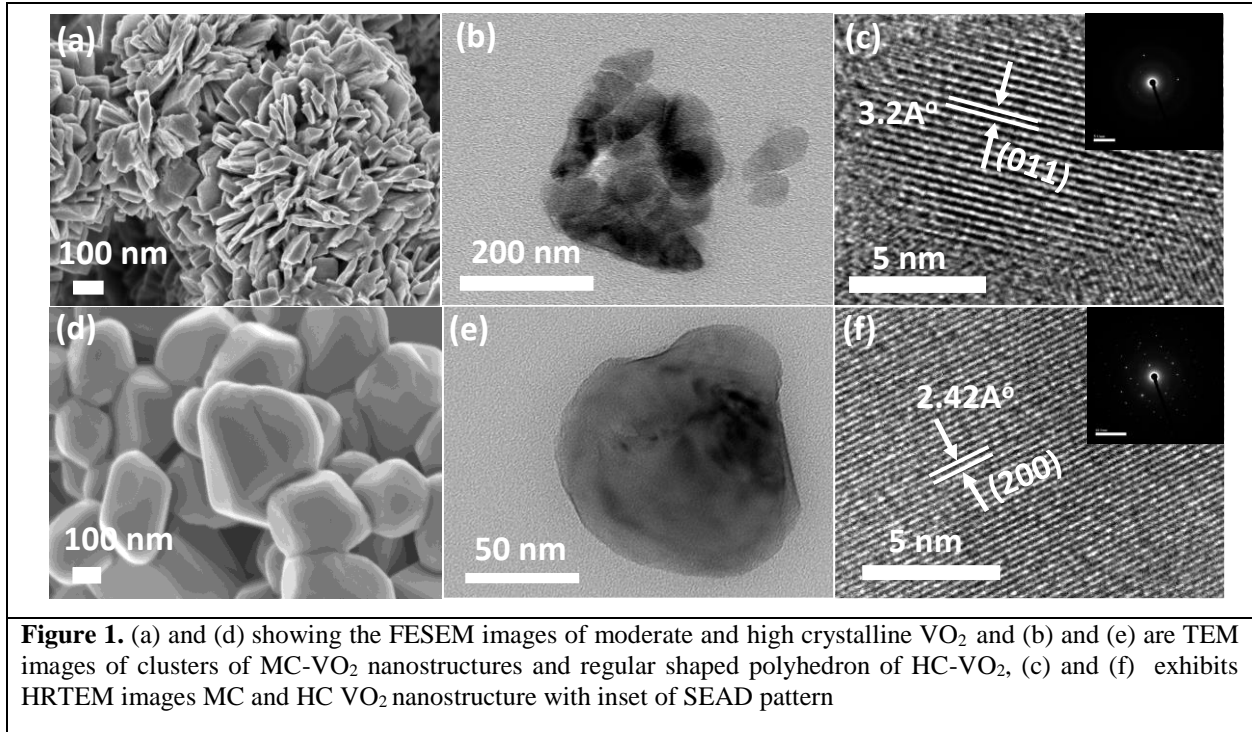
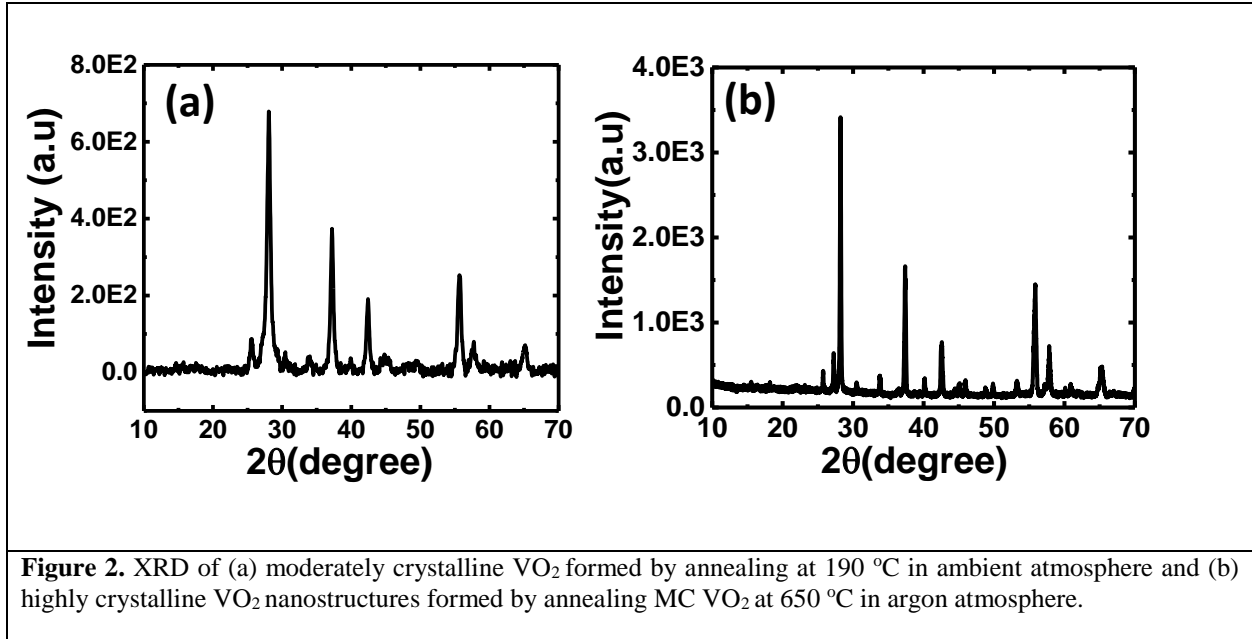
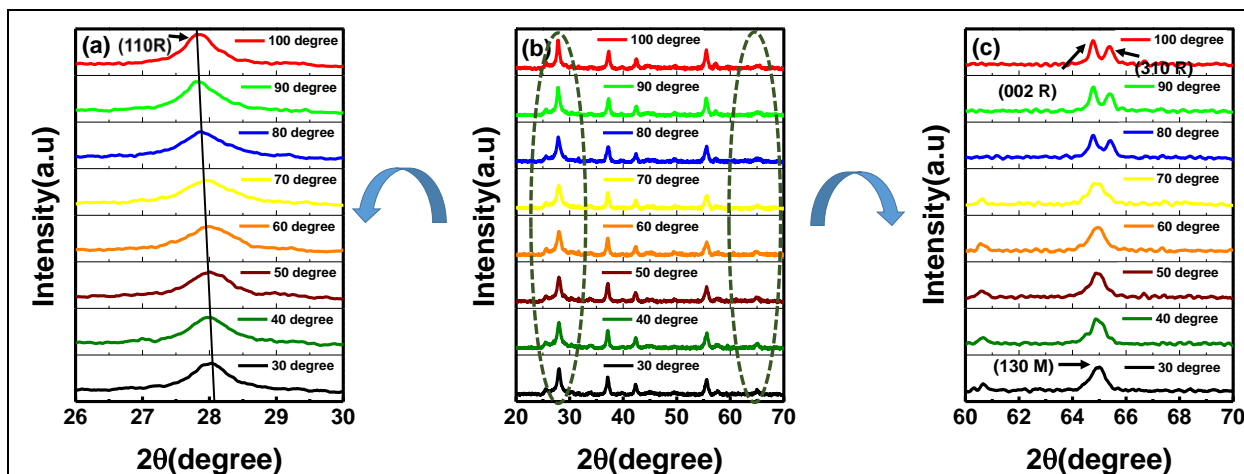


Figure 2(a) and 2(b) clearly shows that the as-prepared VO<sub>2</sub> in both moderate and high crystalline structures were pure for metal to Insulator (MIT) transition.



XRD pattern of as-prepared VEG precursor, with monoclinic phase [JCPDS-49-2497], has highest intensity peak located at  $2\Theta = 13.46^\circ$  in figure S1(b) of supporting information. After thermolysis, VEG peaks started to disappear and started to form MC-VO<sub>2</sub> monoclinic phase with preferred orientation along (011) plane at  $2\Theta = 27.95^\circ$ . As the post annealing temperature is increased further, the XRD peak intensity of VO<sub>2</sub> nanoparticles enhanced considerably with decreased full width half maximum (FWHM), thus obtained HC-VO<sub>2</sub> as shown in Figure 2(b).

Temperature dependent in situ XRD in Figure 3 confirmed the structural phase transition from monoclinic VO<sub>2</sub> (M) to rutile VO<sub>2</sub> (R) phase. Previous reports show that, below the transition temperature of 360 K, XRD pattern matches with (JCPDS-82-0661) data confirming the monoclinic phase, whereas above 360 K rutile phase (JCPDS-79-1655) was confirmed [43]. Shifting of the highest peak in XRD from  $26^\circ \leq 2\Theta \leq 29^\circ$  in figure 3(a) was a clear indication of such structural phase transition in which VO<sub>2</sub> (M) (011) transition into VO<sub>2</sub> (R) (110). Also in Figure 3(c), in the range of  $64^\circ \leq 2\Theta \leq 66^\circ$ , we can observe some splitting of VO<sub>2</sub> (M) (310) peak into two peaks of VO<sub>2</sub> (R) (130) and VO<sub>2</sub>(R) (002).



**Figure 3.** High Temperature XRD of MC-VO<sub>2</sub>. (b) showing the high temperature XRD of moderately crystalline VO<sub>2</sub> in both below and above the metal-insulator transition from VO<sub>2</sub>(M) to VO<sub>2</sub>(R) above 68 °C (a) showing the shift in highest intensity peak in range of 26-30° with temperature (c) showing the gradual splitting of two peaks in range of 62-68° from a single peak at 65°. This confirms the transition of (130) monoclinic plane into two (002) and (310) Rutile planes.

The Same structural transition can be seen in high temperature XRD of HC VO<sub>2</sub> (M) with highest peak shift varies from 26° ≤ 2θ ≤ 29° in Figure 4(a). Two sharp, distinct peaks were also visible in range from 64° ≤ 2θ ≤ 66° in Figure 4(c) above the transition temperature.

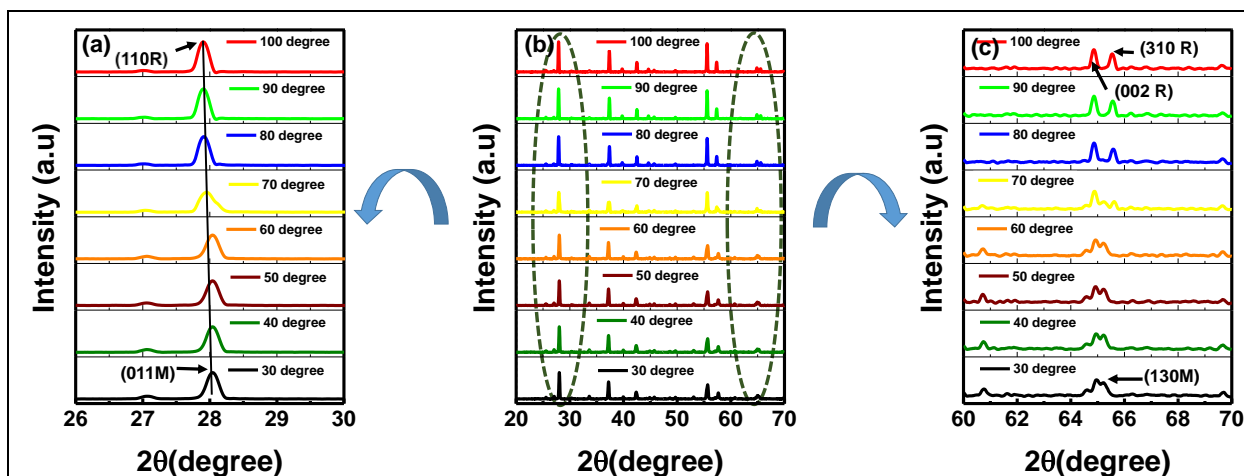
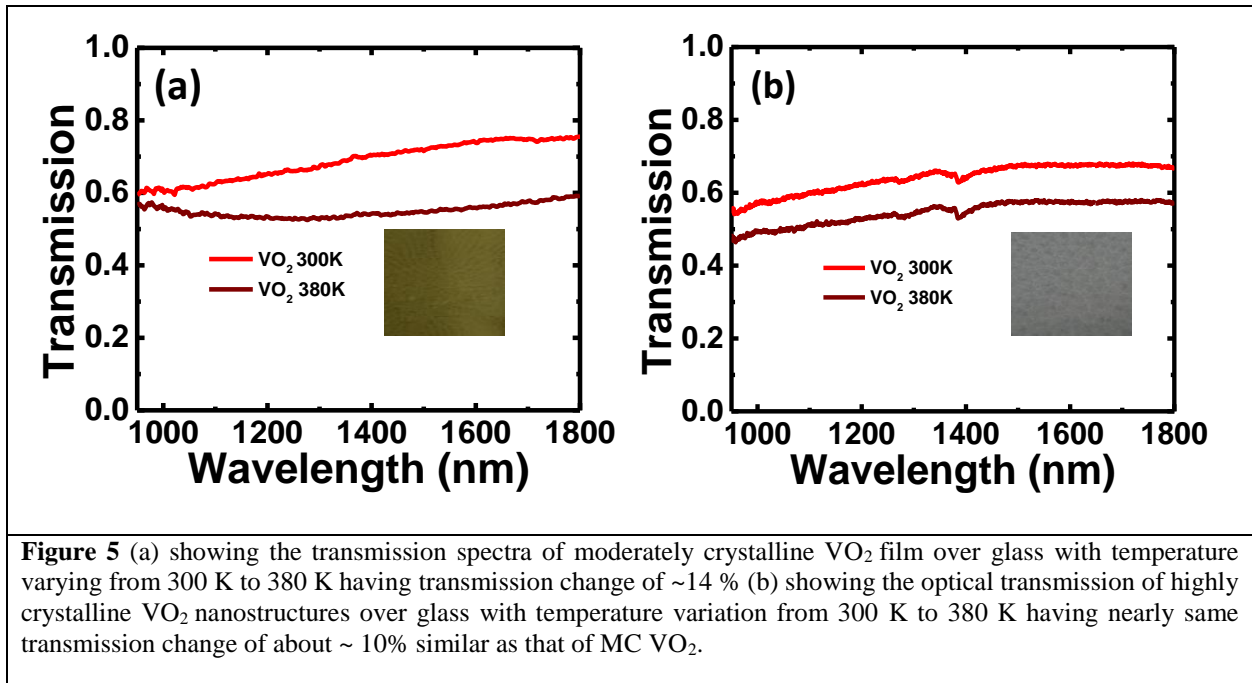


**Figure 4.** High Temperature XRD of HC-VO<sub>2</sub>. (b) showing the high temperature XRD of highly crystalline VO<sub>2</sub> undergoing the transition from VO<sub>2</sub>(M) to VO<sub>2</sub>(R) above 68° C. On the left, (a) showing the shift in highest intensity peak with temperature. (c) showing similar gradual splitting of two peaks in range of 62-68° from a single peak at 65°.

Therefore, temperature dependent XRD establishes the structural phase change following the change in dimension of the unit cell from monocline VO<sub>2</sub> (M) to rutile VO<sub>2</sub> (R). The vanadium atoms with zig zag type atomic orientations in VO<sub>2</sub> (M) results in its characteristic insulating behavior. This shifts to the linear chains of vanadium atom to form VO<sub>2</sub>(R) during the structural transformation above 68 °C.

### 3.2 Optical Characterization

The optical transmission spectra of highly crystalline (HC) and moderately crystalline (MC) VO<sub>2</sub> thin films are shown in Figure. 5(a) and 5 (b).

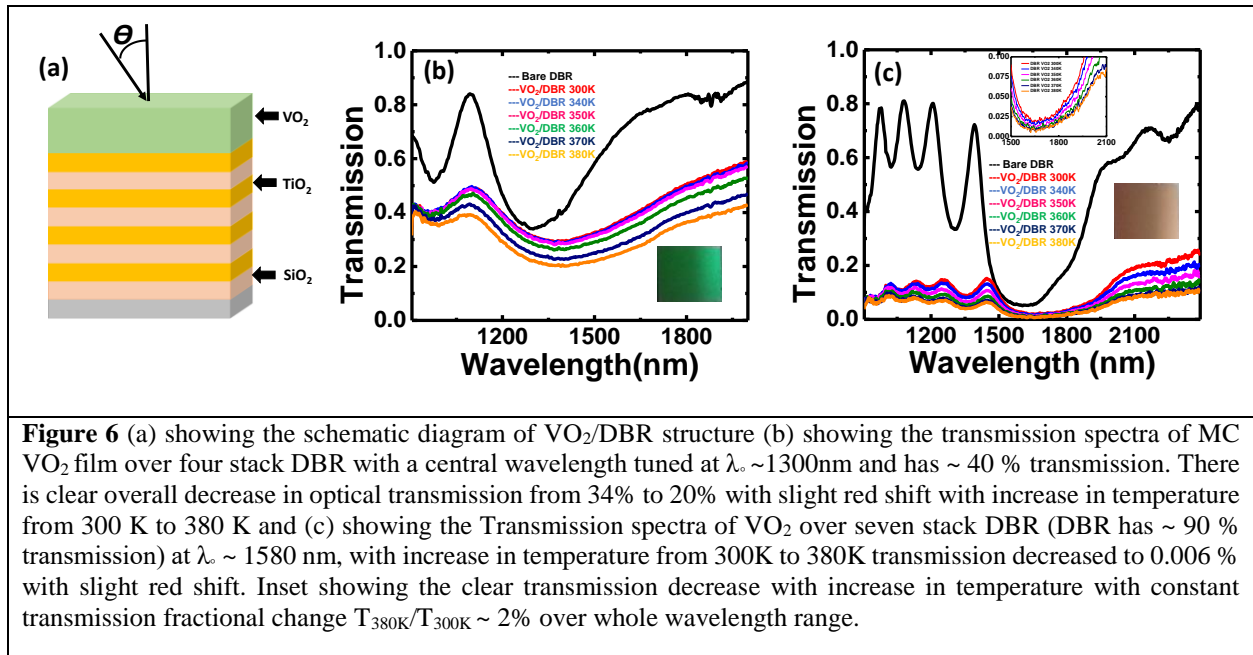


It has been observed that both MC and HC VO<sub>2</sub> films were showing similar kind of transmission reduction with increase in temperature. Both the films were fabricated by drop casting over glass slides and equal amount of VO<sub>2</sub> were taken in all cases. The change in optical transmission is prominent when the temperature increased above 360 K. For MC VO<sub>2</sub> film, with increase in temperature from 300 K to 380 K, optical transmission drops from 67 % to 53 % at 1300 nm and from 73 % to 55 % at 1600 nm. The calculated optical transmission modulation is ( $\Delta T$ ) ~ 14 % at 1300 nm. Similarly HC VO<sub>2</sub> exhibited a similar  $\Delta T$  ~ 10 % at 1600nm when the temperature varies from 300 K to 380 K. The phase structure of VO<sub>2</sub> thin film changed effectively from monoclinic

to rutile above the critical temperature. Xygkis. *et al.* [44] reported a transmission reductions of  $\sim 10\%$  for VO<sub>2</sub> film at 1300 nm, above and below the critical temperature. As both MC and HC are capable of delivering a comparable transmission reduction around the phase transition, hereafter for further studies, we employ MC VO<sub>2</sub>, which provides the advantage of ease of having a synthesis protocol at ambient atmosphere itself.

### 3.2.1 The Fabry-Perot-type optical effect

The Bragg Reflector with VO<sub>2</sub> thin film is fabricated as shown in schematic Figure 6(a). Figure 6(b) showing the optical transmission of 40 % transmitting DBR formed with only four periods of SiO<sub>2</sub>/TiO<sub>2</sub> and tuned at central wavelength  $\lambda_0 \sim 1350$  nm.



On depositing VO<sub>2</sub> layer over DBR, it decreases further to 30 % with a slight shift of 60 nm i.e, from 1350 nm to 1410 nm towards higher wavelengths with  $\sim 25\%$  decrease in optical transmission. This can be attributed towards the enhanced absorption of VO<sub>2</sub> film. With increase in temperature, VO<sub>2</sub> transmission drops downs further to  $\sim 20\%$  at 380 K within the broad wavelength range of 1250-1550 nm. A few periods of Bragg reflector stacks are therefore capable of delivering the desired amount of reduction in optical transmission. Such VO<sub>2</sub>/DBR based hybrid optical absorbers can be effectively used for various thermochromic applications. Consecutively  $\sim 100\%$ , reflecting DBR was also fabricated by increasing the no. of pairs of SiO<sub>2</sub>/TiO<sub>2</sub> stacks as

per equation (2). Here, increasing the number of alternate layers in DBR can increase the reflectivity or by increasing the refractive index contrast between the two alternating layers can increase both reflectivity and bandwidth of the reflector. Therefore, a DBR with nearly 100 % reflectance is fabricated by increasing the no. of stacks of SiO<sub>2</sub>/TiO<sub>2</sub> at central wavelength  $\lambda_0 \sim 1600$  nm from four to seven and it has only  $\sim 0.05$  % optical transmission as demonstrated in Figure 6(c). Therefore, by increasing the no. of layers in the 1D photonic structure one can get nearly 100 % reflectance i.e. effectively a near unity absorption at a desired wavelength.

$$R = [n_o(n_L)^{2N} - n_s(n_H)^{2N} / n_o(n_L)^{2N} + n_s(n_H)^{2N}]^2 \quad (2)$$

When the temperature of VO<sub>2</sub>/DBR ( $\sim 0.05\%$  transmitting) increased to 380 K, its optical transmission further decreased to 0.006 % with a slight spectral red shift to 1668 nm. Thus, it is possible to get almost zero optical transmission or effectively 100 % absorption of VO<sub>2</sub> films. This clearly indicates that the number of stacks (n) of DBR plays very important role in such enhancements. In Figure 6(c), near the stop band, the optical transmission decreases with increase in temperature. However, this not as clearly visible in regions below and above the stop band from the given plot. But the fractional change in transmission  $T_{300K}/T_{380K}$  in the overall range of wavelengths remains nearly same around 2 %. Inset of Figure 6(c) clearly indicates the change in optical transmission with temperature. The slight red spectral shift in both Figure 6(b) and 6(c) may be due to the addition of extra layer of VO<sub>2</sub> (M) over the DBR. This affects the overall optical thickness of the DBR and causes its optical interface pattern to shift slightly to higher wavelength [45]. Another possible reason of such red shift could be the non-uniformity of the VO<sub>2</sub> surface, due to which the effective angle of refraction of light passing through VO<sub>2</sub> layer to DBR deviates towards the lower angles from the normal while entering into DBR as shown in the schematic representation of Figure 6(a). since light entering in DBR from VO<sub>2</sub> is towards a lower angle rather than normal can cause the red spectral shift which is shown by the Matlab simulation program based on the transfer matrix method (code given in supporting information) to calculate the spectral coefficients of this multilayered structure, as per equation (3) represents the reflection and transmission coefficients of a DBR can be obtained by Fresnel expressions,

$$R_s = [(n_o - n_1) / (n_o + n_1)]^2, T_s = [4n_o n_1 / (n_o + n_1)^2] \quad (3)$$

Where  $R_s$  is the reflection coefficient and  $T_s$  is the transmission coefficient. If  $M_T$  represents the product of transfer characteristic matrices and  $M_i = 1, 2$  represents individual layers in the Bragg

reflector. And  $M_{VO_2}$  represents Matrix corresponds to  $VO_2$  layer, then final the transfer characteristic matrix is given as,

$$M_T = M_{VO_2} * (M_1 * M_2 * M_1 * M_2 * \dots * M_n)^{q/2} \quad (4)$$

Where  $q$  is the number of stacks [46]. Calculating this transfer matrix for non-normal angle of incidence shows prominent red shift when light refract towards a lower angle.

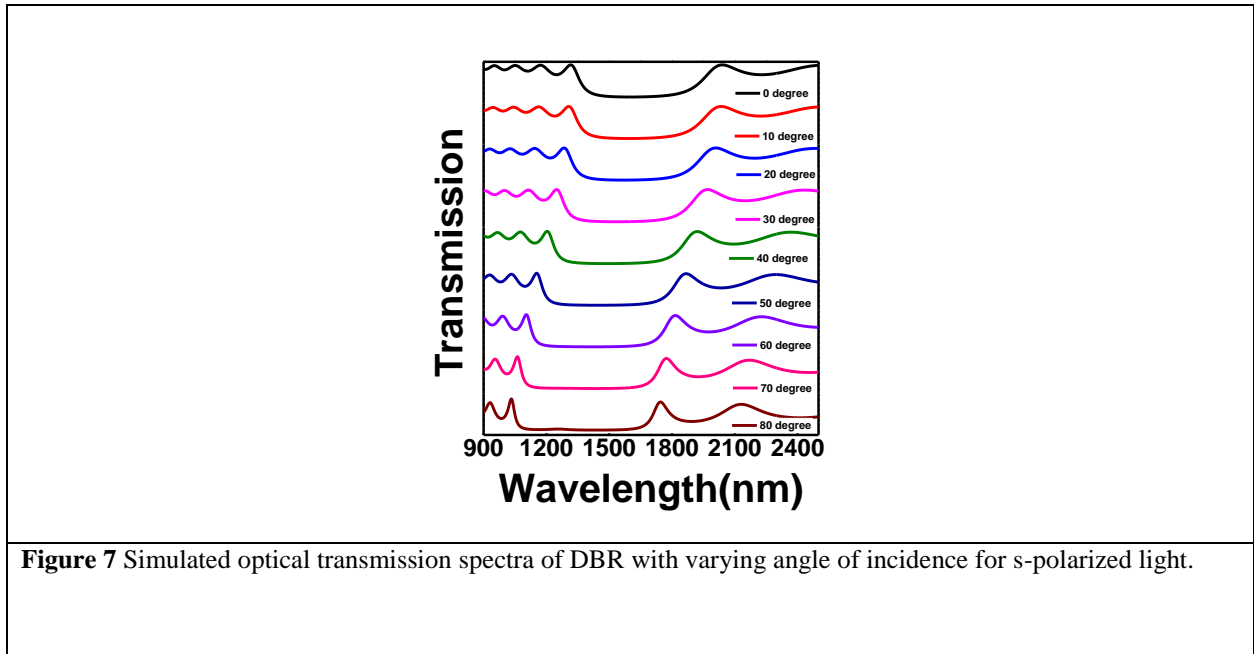


Figure 7, depicts the simulation results of such red spectral shift in  $VO_2$ /DBR structure when light incident at lower angles [46] and following equations 3 and 4, here in the program, we are considering that angle dependence transmissivity has negligible scattering loss, thus giving a red shift with a decrease in angle of incidence for s-polarized light in a  $VO_2$ /DBR structure. Therefore, it is also likely that some non-uniformity of the  $VO_2$  surface may also cause such changes in the effective angle of refraction of light passing from the  $VO_2$  thin films into the DBR which causing the red spectral shift of the whole transmission spectra.

## Conclusion

In summary, VO<sub>2</sub> (M) was synthesized by thermolysis of vandyl complex at 190 °C in ambient atmosphere which yields MC VO<sub>2</sub> (M) nanostructures. Post annealing treatment at 650 °C under argon atmosphere results highly crystalline VO<sub>2</sub> (M). High temperature XRD clearly confirms the crystal phase change from monoclinic to rutile above 68 °C for both MC and HC VO<sub>2</sub>. Both these films exhibit almost similar transmission reductions (~ 10 %) due to structural phase change above their metal-insulator transition temperature. Therefore, MC VO<sub>2</sub> has been employed for further studies due to its ease of synthesis at ambient atmospheric conditions without any post-growth annealing steps. By depositing VO<sub>2</sub> over DBR with four periods of SiO<sub>2</sub>/TiO<sub>2</sub> exhibits ~ 20 % transmission change. Upon increasing the temperature, effective absorption enhanced considerably. On increasing the number or periods of SiO<sub>2</sub>, TiO<sub>2</sub> to seven, results in the formation of a DBR having a stop band at 1600 nm with ~ 0.05 % transmission. By depositing VO<sub>2</sub> over a good quality DBR leads to ~ 100 % reduction in optical transmission over a certain wavelength region in IR. Hence such hybrid structures are potential candidates for designing VO<sub>2</sub> based optical absorbers for various thermochromic applications such as smart windows and IR sensors. Further work is going on to tailor these hybrid VO<sub>2</sub> nanoparticles and ID photonic crystal structure to lower metal-insulator transition temperature of 68 °C towards room temperature with suitable doping for ambient operations.

## Acknowledgements

RN acknowledges funding from the Department of Science Technology, India through INSPIRE faculty scheme (DST/INSPIRE/04/2017/002761). We also acknowledge the support from Department of Science and Technology, India (Research Grant SR/NM/TP13/2016). We also thank Dr. Shouvik Datta (IISER Pune) for valuable discussion.

## References

1. Rajeswaran B, Pradhan J K, Ramakrishna S A and Umarji A M 2017 Thermochromic VO<sub>2</sub> thin films on ITO-coated glass substrates for broadband high absorption at infra-red frequencies *J. Appl. Phys.* **122** 163107

2. Cao Z, Xiao X, Lu X, Zhan Y, Cheng H and Xu G 2016 A simple and low-cost combustion method to prepare monoclinic VO<sub>2</sub> with superior thermochromic properties *Sci. Rep.* **6** 39154
3. Wu C, Feng F and Xie Y 2013 Design of vanadium oxide structures with controllable electrical properties for energy applications *Chem. Soc. Rev.* **42** 5157
4. Xiao X, Cheng H, Dong G, Yu Y, Chen L, Miao L and Xu G 2013 A facile process to prepare one dimension VO<sub>2</sub> nanostructures with superior metal–semiconductor transition *Cryst. Eng. Comm.* **15** 1095
5. Zhang Z, Gao Y, Chen Z, Du Z, Cao C, Kang L and Luo H 2010 Thermochromic VO<sub>2</sub> Thin Films Solution-Based Processing, Improved Optical Properties, and Lowered Phase Transformation Temperature *Langmuir* **26** 10738
6. Shao Z, Cao X, Luo H and Jin P 2018 Recent progress in the phase-transition mechanism and modulation of vanadium dioxide materials *NPG Asia Materials* **10** 581
7. Fan L, Chen Y, Liu Q, Chen S, Zhu L, Meng Q, Wang B, Zhang Q, Ren H and Zou C 2016 Infrared Response and Optoelectronic Memory Device Fabrication Based on Epitaxial VO<sub>2</sub> Film. *ACS Appl. Mater. Interfaces* **8** 32971
8. Zhou J, Gao Y, Zhang Z, Luo H, Cao C, Chen Z, Dai L and Liu X 2013 VO<sub>2</sub> thermochromic smart window for energy savings and generation *Sci. Rep.* **3** 3029
9. Xu F, Cao X, Luo H and Jin P 2018 Recent advances in VO<sub>2</sub>-based thermochromic composites for smart windows *J. Mater. Chem. C* **6** 1903
10. Pradhan J K, Ramakrishna S A, Rajeswaran B, Umarji A M, Achanta V G, Agarwal A K and Ghosh A 2017 High contrast switchability of VO<sub>2</sub> based metamaterial absorbers with ITO ground plane *Opt. Express* **25** 911
11. Song Z, Wang K, Li J, and Q H Liu 2018 Broadband tunable terahertz absorber based on vanadium dioxide metamaterials *Opt. Express* **26** 7148
12. Song S, Ma X, Pu M, Li X, Guo Y, Gao P and Luo X 2018 Tailoring active color rendering and multiband photodetection in a vanadium-dioxide-based metamaterial absorber *Photonics Res.* **6** 492
13. Zamani N, Hatef A, Nadgaran H and Keshavarz A 2017 Control of electromagnetically induced transparency via a hybrid semiconductor quantum dot–vanadium dioxide nanoparticle system *J. Nanophoton.* **23** 036011
14. Joannopoulos J D, Johnson S G, Winn J N, Meade R D 2011 Photonic crystals: molding the flow of light Princeton university press
15. Muallem M, Palatnik A, Nessim G D, and Tischler Y R 2014 Room Temperature Fabrication of Dielectric Bragg Reflectors Composed of a CaF<sub>2</sub>/ZnS Multilayered Coating *ACS Appl. Mater. Interfaces* **7** 474
16. Schubert M F, Xi J Q, Kim J K, and Schubert E F 2007 Distributed Bragg reflector consisting of high- and low-refractive-index thin film layers made of the same material *Appl. Phys. Lett.* **90** 141115
17. Anaya M, Rubino A, Calvo M E and Miguez H 2016 Solution processed high refractive index contrast distributed Bragg reflectors *J. Mater. Chem. C.* **4** 453

18. Lu Y J, Shan C X, Jiang M M, Li B H, Liu K W, Li R G and Shen D Z 2014 Enhanced Emission from ZnO- based double heterostructure light-emitting devices using a distributed Bragg reflector *RSC Adv.* **4** 1657
19. Lin S Y and Fleming J G 2003 Origin of absorption enhancement in a tungsten, three-dimensional photonic crystal *J. Opt. Soc. Am.* **20** 153
20. Iasilli G, Francischello R, Lova P, Silvano S, Surace A, Pesce G, Alloisio M, Patrini M, Shimizu M, Comoretto D and Pucci A 2019 Luminescent solar concentrators: boosted optical efficiency by polymer dielectric mirrors *Mater. Chem. Front.* **3** 429
21. Park Y, Drouard E, Daif O E, Letartre X, Viktorovitch P, Fave A, Kaminski A, Lemiti M, Seassal C 2009 Absorption enhancement using photonic crystals for silicon thin film Solar cells, *Opt. Express* **17** 14312
22. Mbakop F K, Djongyang N and Raïdandi D 2016 One-dimensional TiO<sub>2</sub>/SiO<sub>2</sub> photonic crystal filter for thermophotovoltaic applications *J. Eur. Opt. Soc. Rapid.* **12** 23
23. Atwater H A and Polman A 2010 Plasmonics for improved photovoltaic devices *Nature Mater.* **9** 205
24. Fahr S, Rockstuhl C and Lederer F 2009 Metallic nanoparticles as intermediate reflectors in tandem solar cells *Appl. Phys. Lett.* **95** 121105
25. Barve A V, Lee S J, Noh S K, and Krishna S, 2010 Review of current progress in quantum dot infrared photodetectors *Laser Photon. Rev.* **4** 738
26. Inan H, Poyraz M, Inci F, Lifson M A, Baday M, Cunningham B T, and Demirci U 2010 Photonic crystals: emerging biosensors and their promise for point-of-care applications *Chem. Soc. Rev.* **46** 366
27. Pitruzzello G and Krauss T F 2018 Photonic crystal resonances for sensing and imaging *J. Opt.* **20** 073004
28. Adl H P, Bayat F, Ghorani N, Kandjani S A and Tajalli T 2016 A Defective 1-D Photonic Crystal-Based Chemical Sensor in total Reflection Geometry *IEEE Sensors Journal* **17** 4046
29. Beregovski Y, Hennig O, Fallahi M, Guzman F, Clemens R, Mendes S and Peyghambarian N 1998 Design and characteristics of DBR-laser-based environmental sensors *Sens.Actuators* **53** 116
30. Devarapu G C R and Foteinopoulou S 2012 Mid-IR near-perfect absorption with a SiC photonic crystal with angle-controlled polarization selectivity *Opt. Express* **20** 13041
31. Fu S M, Zhong Y K, Tu M H, Chen B R and Lin A 2016 A fully functionalize metamaterial perfect absorber with simple design and implementation *Sci. Rep.* **6** 36244
32. Hajian H, Ghobadi A, Butun B, and Ozbay E 2017 Nearly perfect resonant absorption and coherent thermal emission by hBN-based photonic crystals *Optics Exp.* **25** 31970
33. Cao J, Wang J, Yang G, Lu Y, Sun R, Yan P and Gao S, 2017 Enhancement of broadband light absorption in monolayer MoS<sub>2</sub> using Ag grating hybrid with distributed Bragg reflector *Superlattices Microstruct.* **110** 26
34. Zhou K, Song J, Lu L, Luo Z, and Cheng Q 2019 Plasmon-enhanced broadband absorption of MoS<sub>2</sub>-based structure using Au nanoparticles *Opt. Express.* **27** 2305
35. Lu Y, Yang G, Xue J, Wang J, Zhang X, Yan X and Hua B 2018 Magnetic polariton

- Enhanced broadband absorption and photoresponse of monolayer MoS<sub>2</sub> based on normal and anomalous metallic gratings *J. Phys. D: Appl. Phys.* **51** 295104
36. Vincenti M A, Ceglia D D, Grande M, D’Orazio A and Scalora M 2013 Nonlinear control Of absorption in one-dimensional photonic crystal with graphene-based defect , *Opt. Lett.* **38** 3550
  37. Wang X, Liang Y, Wu L, Guo J, Dai X and Xiang Y 2018 Multi-channel perfect absorber based on a one-dimensional topological photonic crystal heterostructure with graphene, *Opt. Lett.* **43** 4256
  38. Zhu M, Qi H, Wang B, Wang H, Zhang D and Lv W 2018 Enhanced visible transmittance and reduced transition temperature for VO<sub>2</sub> thin films modulated by index-tunable SiO<sub>2</sub> anti- reflection coatings *RSC Adv.* **8** 28953
  39. Rashidi A, Hatef A and Namdar A 2018 On the enhancement of light absorption in vanadium dioxide/1D photonic crystal composite nanostructures *J. Phys. D: Appl. Phys.* **51** 375102
  40. Rashidi A, Hatef A, and Namdar A 2018 Modeling photothermal induced bistability in vanadium dioxide/1D photonic crystal composite nanostructures *Appl. Phys. Lett.* **113** 101103
  41. Zou J, Peng Y and Lin H 2013 A low-temperature synthesis of monoclinic VO<sub>2</sub> in an atmosphere of air *J. Mater. Chem. A.* **1** 4250
  42. Xiao X, Zhang H, Chai G, Sun Y, Yang T, Cheng H, Chen L, Miao L and Xu G 2014 A cost-effective process to prepare VO<sub>2</sub> (M) powder and films with superior thermochromic properties *Mater. Res. Bull.* **51** 6
  43. Wu C, Zhang X, Dai J, Yang J, Wu Z, Wei S and Xie Y 2011 Direct hydrothermal synthesis of monoclinic VO<sub>2</sub>(M) single-domain nanorods on large scale displaying magnetocaloric effect, *J. Mater. Chem.* **21** 4509
  44. Xygkis M, Gagaoudakis E, Zouridi L, Markaki O, Aperathitis E, Chrissopoulou K, Kiriakidis G and Binas V, 2019 Thermochromic Behavior of VO<sub>2</sub>/Polymer Nanocomposites for Energy Saving Coatings *Coatings* **9** 163
  45. Lova P 2018 Selective Polymer Distributed Bragg Reflector Vapor Sensors *Polymers* **10** 1161
  46. Leem J W, Guan X Y and Yu J S 2014 Tunable distributed Bragg reflectors with wide angle and broadband high-reflectivity using nanoporous/dense titanium dioxide film stacks for visible wavelength applications *Opt. Express* **22** 18519

